Jurnal Tribologi 33 (2022) 80-96

Jurnal Tribologi
Website : jurnaltribologi.mytribos.org e-issn: 2289-7232

The effect of tensile strength and surface roughness by varying oxygen level in 3D printer chamber

Muhammad Arifuddin Che Mat [1], Faiz Redza Ramli [1,2*], Mohd Nizam Sudin [1,2], Safarudin Ghazali Herawan [3], Mohd Rizal Alkahari [1,2]

[1] Fakulti Kejuruteraan Mekanikal, Universiti Teknikal Malaysia Melaka, Hang Tuah Jaya, 76100 Durian Tunggal, Melaka, MALAYSIA.
[2] Centre for Advanced Research on Energy, Universiti Teknikal Malaysia Melaka, Hang Tuah Jaya, 76100, Durian Tunggal, Melaka, MALAYSIA
[3] Faculty of Engineering, Bina Nusantara University, 11480 Jakarta, INDONESIA.
*Corresponding author: faiz@utem.edu.my

KEYWORDS

Fused filament fabrication
3D printer
Surface roughness
Layer thickness
Oxygen exclusion

ABSTRACT

The part produced by the fused filament fabrication (FFF) 3D printer in terms of surface roughness, tensile strength, and dimensional accuracy depends mainly on the printing parameters and the environmental printing conditions. In this paper, nitrogen gas had been allowed to flow inside the 3D printer chamber to maintain an inert environment and to remove the rate of concentration oxygen inside the chamber. This paper is devoted to studying the influence of layer thickness and surface roughness on the mechanical properties of 3D-printed parts. Tensile and surface roughness tests were performed on samples of three different layer thicknesses (0.1mm, 0.2mm, and 0.3mm) using an Acrylonitrile Butadiene Styrene (ABS) in (FFF) 3D printing method. Therefore, the results explain the oxygen ambient is 10.295 (MPa) at the 0.1mm layer thickness for the tensile test, which is weaker than nitrogen ambient of 11.767 (MPa). The scanning electron microscope (SEM) observed a strong bonding with microstructure (fewer deficiencies and voids) for 0% oxygen, compared to 10% and 20% with the large void area.

Received 30 November 2021; received in revised form 22 February 2022; accepted 14 April 2022.
To cite this article: Ramli et al. (2022). The effect of tensile strength and surface roughness by varying oxygen level in 3D printer chamber. Jurnal Tribologi 33, pp.80-96.

1.0 INTRODUCTION

Additive Manufacturing (AM), or the commonly used term 3D printer, is a layer-by-layer fabrication of geometric three-dimensional (3D) shapes based on design CAD data. One of the first additive manufacturing (AM) methods was rapid prototyping. Commercially available additive manufacturing (AM) innovations include stereolithography (STL) (Balashanmugam et al., 2014), selective laser sintering (SLS) (Fina et al., 2017), inkjet printing (IJP) (Derby, 2011), direct metal deposition (DMD) (Yan et al., 2017), and fused deposition modeling (FDM) (Alafaghani et al., 2017). An extensively used rapid prototyping technique involving fused deposition modeling (FDM), also known as fused filament fabrication (FFF), has been around since the 1980s. (Diegel et al., 2016). Besides, this technique makes it possible to create parts with complex geometries, which are challenging to produce using traditional manufacturing methods. Similarly, final geometries allowed by AM technologies can also improve the quality or production (Quadrennial Technology Review, 2015).

3D objects manufactured by FFF are gradually advanced by better processing parameters such as a reduced layer resolution or a construct orientation (Hossain et al., 2014). As illustrated in Figure 1, the FFF manufacturing process utilizes a circular nozzle, typically 1.75 mm in diameter, that transverses in the x and y planes through a multi-speed numerically controlled mechanism to generate each two-dimensional (2D) layer of approximately 20 m to 300 m (depending on the 3D printer and process parameters) and extrudes them from a spool (Yuen, 2016). The spooled thermoplastic filament materials are fed into the liquefier through a pair of counter-rotating mechanical freewheels, which apply enough torque to the thermoplastic filament material to act as a piston during the extrusion stage and then deposit it layer by layer or path by path onto an adjustable build plate based on the 3D computer-aided design (CAD) model (Wang et al., 2007). The create platform pushes in the Z-direction and begins the deposition of a new layer while maintaining a constant X-Y coordinate in the X-Y plane when the 3D printed sample has reached its target position. For a while, the print head nozzle would have deposited an exact physical image of the three-dimensional (3D) computer-aided design (CAD) design file (Ahn et al., 2002).

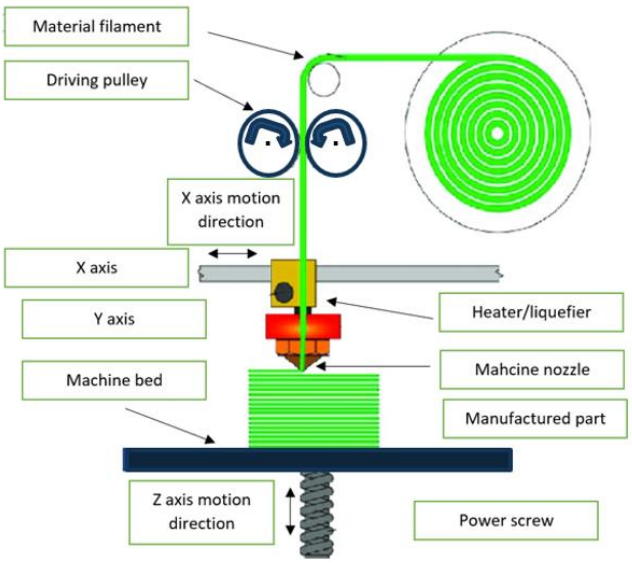

Figure 1: Flow process and principal components of fused filament fabrication.

Furthermore, as the ability to withstand deformation under load-printed components, flexural strength is an essential aspect of FFF technology that enables the features to work longer. Different FFF machine parameters such as layer thickness, infill density, pattern, and raster angle give different finishing quality to the final shape (Nazan et al., 2017). Many scholars have investigated the impact of various parameters on printed mechanical rates (Quan et al., 2018). It was concluded that a minimum layer thickness, an orientation of zero, maximum raster angle and width, and negative air gap yields the highest mechanical strength (Norani et al., 2021). Thus, essential questions arise, such as whether the surface roughness is influenced by FFF machine parameters, materials, and environments. Additionally, the layer thickness is a critical parameter that affects the FFF responses. The layer thickness of most FFF machines is approximately 0.254 mm (Gibson et al.,2020)

Acryl-butadiene-styrene (ABS) is one of the products commonly used to manufacture additives. It is a high strength, toughness, and easy to process opaque thermoplastic polymer. Extrusion is the most common method for producing ABS products. It has good resistance and toughness, but the properties can differ according to the final processing conditions, such as temperature and processing method. However, a finished product's properties are controlled, rather than its material properties, by various parameters such as raster direction, air gap, binding saturation, and layer thickness (Shubham et al., 2016). The performance of the FFF parts became of primary consideration to the manufacturer and users, and the characteristics of the FFF part, such as tensile strength, flexural strength, compressive strength, dimensional accuracy, surface roughness, build time, yield strength, and ductility, are often being discussed (Buj-Corral et al., 2019). One of the drawbacks of AM, especially in the fused filament fabrication (FFF) process, is that the printed part's surface roughness is excessively rough due to layer-by-layer deposition (Alsoufi & Elsayed, 2017). Nur et al. (2018)found that degradation processes in the presence of oxygen can lead to a decrease in molecular weight compared to the printing process carried out under the strict exclusion of oxygen.

Therefore, environmental factors such as oxygen exposition and temperature might also influence filament degradation factors (Nur et al., 2018). Lederle et al., (2016) treated the fused deposition modelling (FDM) 3D print with nitrogen gas and observed a significant increase in elongation at break and a 30% increase in tensile strength for both ABS and PLA specimens. The improved mechanical properties were achieved by suppressing the oxidation process, which reduced polymer surface degradation and improved layer adhesion. Maidin et al., (2018) used the FDM process to print an ABS sample in a vacuum chamber. As a result of the lack of blobs and stringing, the surface became much smoother. It was also discovered that the staircase effect was significantly reduced, while the surface smoothness was improved by 9 percent when compared to the standard print sample. Although it improves flexural strength, it is not suitable for applications requiring higher tensile strength. Ferrar et al., (2012) expected that the manner of delivering inert gas flow across the build platform will have a substantial impact on the quality and reproducibility of components across the build area. This gas flow is largely utilised to keep the requisite inert environment in place during processing. The improved gas flow had a substantial effect on both the value and the standard deviation of the measured attributes, with porosity decreasing by 1.7 percent and the standard deviation of compression strength improving from 12 MPa to 5 MPa. Li & Cai, (2011) discovered that when carbon fibers (CF) was treated with HNO3, the bond strength with the ABS and polyamide-6 matrices increased. Montes-Morán et al., (2001) subjected CF to oxygen plasma treatment and discovered that the link between CF and the PC matrix was significantly enhanced, resulting in increased interlaminar shear strength.

Several studies have been conducted over the last few years to improve the mechanical properties, and aesthetic value of the FFF printed part by acceptable process parameters. However, the findings did not focus on the techniques designed to improve the 3D printed part's quality. Due to specific factors, specific oxidation processes occurring in polymers contribute to substance degradation at higher temperatures in the presence of oxygen. Consequently, each layer's polymer surface is vulnerable to degradation during the FFF process affecting the mechanical properties. The breakdown of different polymers at higher temperatures has been extensively studied. In most situations, the polybutadiene stage (which involves the active two-fold bonding) is affected by oxidation reactions, which result in a highly significant reduction in mechanical properties (Lederle et al., 2016). Many different materials can be used for FFF, such as thermoplastic polyester, polyamide, wax, and metal, to obtain various final shapes and appearances (Alsoufi & Elsayed, 2017).

Surface finish quality is crucial for improved functionality, ergonomics, appearance, and overall prototype time reduction. Pérez et al., (2018) consider layer height, printing speed, temperature, printing path, and wall thickness, layer height and wall thickness were discovered to have the largest influence on arithmetical mean height, $R_{a.}$ (Reddy et al., 2018) examined build inclination as well as layer thickness, material infill, and printing quality. Furthermore, the FFF systems manufacturing capability regarding the printed part's mechanical properties has not achieved the criteria as good quality as the other AM technology. Despite its advantages and success, the widespread adoption of additive manufacturing is hindered by poor mechanical properties, a lack of successful part printing, and AM skills (D'Amico et al., 2017). FFF provides a wide variety of products with efficient mechanical properties for printed pieces. However, the printing speed is low, and the component structure contributes to poor surface roughness due to the escalating effect (Buj-Corral et al., 2019). The main disadvantages are surface quality (Gajdoš et al., 2015), the need of support structures, axial weakness perpendicularly, a larger area of slices requires longer building times, and temperature fluctuations during production could lead to delamination, and high surface roughness.

Several works based on the stair-stepping result demonstrate that the bigger the layered thickness, would lower surface roughness (Galantucci et al., 2010). After all, there is still no best choice of process parameters for all kinds of materials. However, part accuracy develops on AM techniques and has led to significant research problems. Optimization of the process parameter is a considerable challenge for accuracy, roughness and finishing, and fabrication time for development (Galantucci et al., 2015). Although decreasing layer thickness improves the surface roughness of prototypes produced on 3D printing machines, this issue is also influenced by the angle between the vertical axis and the surface tangents (staircase effect). In the case of FDM, the width of the road, the air gap between the roads, and the model temperature all have an effect on the surface roughness. However, the demand for efficient use of this technology for producing fine details, high strength parts with low dimensional variation, and suitable surface quality is growing(Vaezi & Chua, 2011).

This experiment aims to study the significant effect on tensile strength and surface roughness when varying the different oxygen concentrations during printing the samples. FFF components often appear to have anisotropic mechanical properties because of the layer-by-layer fabrication process. We briefly compare FFF-printed parts under standard operating conditions to those printed under strict oxygen exclusion. We demonstrate a noticeable improvement in mechanical properties such as yield strength when the print is conducted inside an enclosed chamber. The enhanced properties of parts printed under inert gas conditions were discovered during the

direct print of reaction vessels for extremely oxygen- and water-sensitive substances in a nitrogen atmosphere. The method described here could result in a relatively straightforward enhancement of FFF printers.

2.0 EXPERIMENTAL PROCEDURE

2.1 3D Printing Setup

The 3D printer machine used for this experiment is an open-source fused filament fabrication Anet A8 (do-it-yourself kit), which is very commonly available in the market and easy to use with low maintenance cost. Besides, to avoid oxygen from being environmentally safe, the 3D printer system was within an enclosed chamber of (550 x 550 x 450) mm^3, as seen in Figures 2. Nitrogen gas could flow through an inlet pipeline into the enclosed chamber to fill the gas inside the environment. The enclosed chamber was operated under nitrogen with a pressure of +5 bar (vs atmospheric pressure) and a flow rate of 12 m^3 h^{-1}. An oxygen detector of the Uyigao brand and model UA6070B was used to ensure the percentage concentration of oxygen within the chamber while the gas was flowing out by nitrogen. This process takes several minutes to flow out at the specific oxygen content level inside the enclosed chamber. Besides, an enclosed chamber was placed into the fume cupboard to capture and remove harmful chemicals released into the air during the experiments. Therefore, both inlet and the outlet of the chamber were closed after the oxygen was removed. In the enclosed chamber, this experiment was repeated using different Nitrogen gas levels, 0%, 10%, and 20% oxygen.

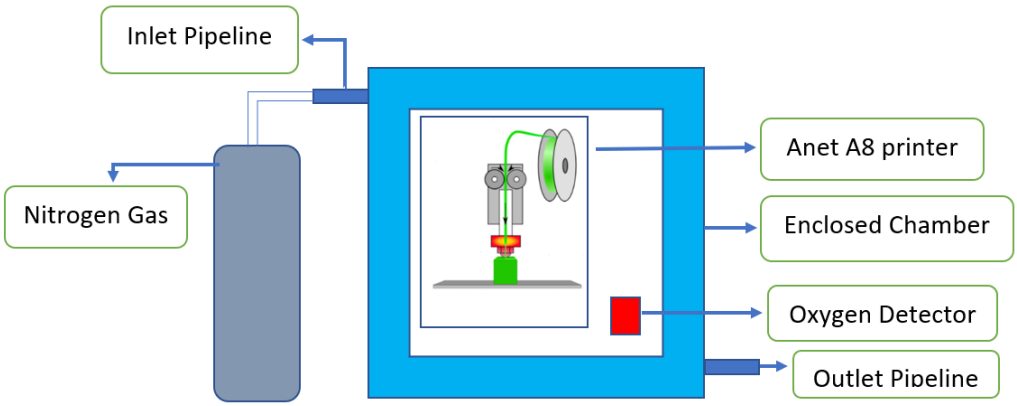

Figure 2: Schematic diagram for the FFF machine inside the chamber.

2.2 Sample Preparation

Five acceptable specimen forms in ASTM D638 vary in size according to the specimen's thickness and the available material. The most frequently used specimens are Type I specimens, which have a thickness of 3.2 mm and are typically fabricated using an open-source Anet A8 printer. Type I specimens measure 165 mm in length and 13 mm in width, with a gauge length of 50 mm. Figure 3 was prepared according to the geometry and dimensions specified in ASTM D638 type I Standard Test Method for Tensile Properties of Plastics (N. Searle, 2014). The dog-bone

specimen was designed using Solidworks, and thus it was exported in an STL format. Figure 3 shows the sample dog bone of ABS tested using Universal testing machine Instron 8872. Type I ASTM D638 was chosen for this experiment because it is more suitable for this dog bone sample than type IV.

Besides, the solid model is converted into STL by software version Repetier-Host V.1.0.5. The specimens will set up the parameter using this software to modify the G-code parameter before 3D printing starts reading the file. Dog bone samples were printed with four samples simultaneously and would replicate with different parameter settings in the duration printer. Since this work's main goal was to investigate the printing process's adhesion, the specimen was placed with the longest side orthogonal to the printing and the shortest side parallel to the platform's moving path (printing) surface (perpendicular) to maximize the number of layers. The mechanical properties of the printing path have been studied in great depth (Searle, 2014). This software can also easily predict the time needed to complete a single sample.

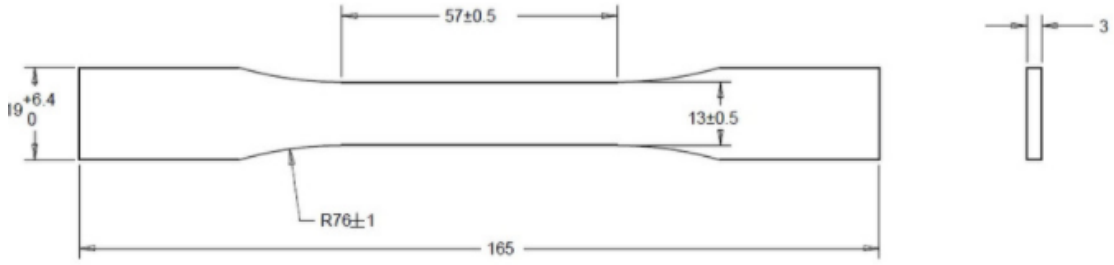

Figure 3: ASTM D638 – Type I Standard test method for tensile properties of plastic.

Table 1: Summary of the operating setup of the 3D printer.

Number of Parameters	Processing Parameter	Value Used
1	Material used	ABS (Acrylonitrile Butadiene Styrene)
2	Temperature (°C)	240
3	Infill pattern Linear	Honeycomb
4	Speed (mm/s)	30
5	Level of Oxygen contains in the chamber (%)	0, 10, 20
6	Layer thickness (mm)	0.1, 0.2, 0.3
7	Infill design %	0
8	Raster angle	90º

In Table 1, the layer thickness selection of 0.1, 0.2, and 0.3 is the optimal thickness from the previous research study. Meanwhile, it is most likely used in regular FFF applications for an infill density of 0% (Alsoufi & Elsayed, 2017). One of the crucial factors to be considered in 3D printing can radically influence the build time. The infill density for FFF 3D printed parts is kept as low as possible to save print time and content. As a result, the infill density was set to 0%. The raster angle is the angle provided for filament deposit, so the 90-degree angle was selected to observe

the deposited filament arrangement when using the 3D contact non-profilometer. Generally, the process parameter selection depends on using a 3D printer because it is necessary to determine the desired mechanical properties.

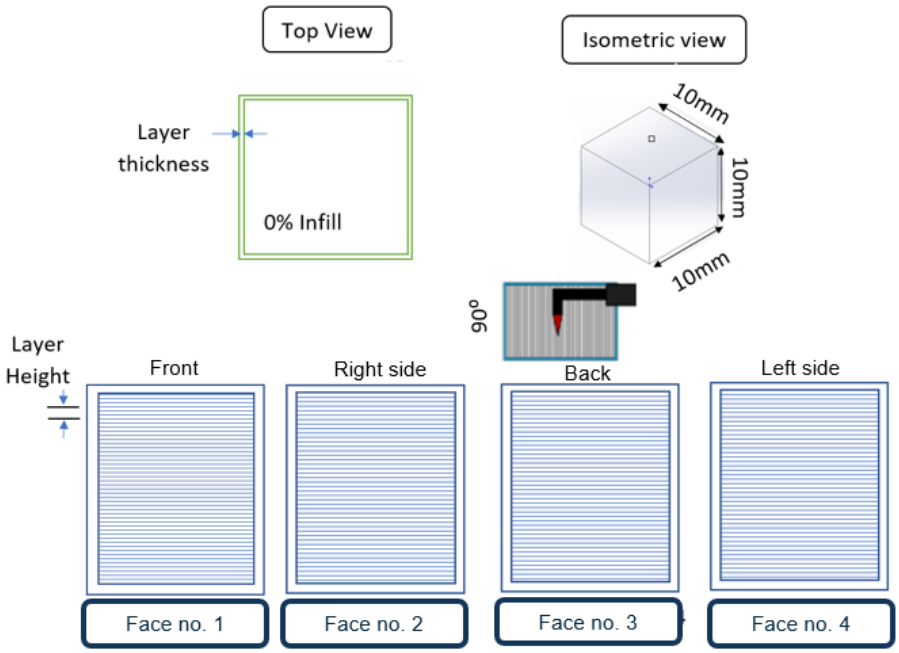

Figure 4: The proposed framework of the 0% infill density of geometry block with four different faces.

Figure 4 shows the framework for the surface roughness test for a simple geometry block with measurements of 10 mm (L) × 10 mm (W) × 10 mm (H) square was fabricated using the 3D printer machine. This size is selected due to reducing the amount and reducing the cost of producing parts. Therefore, this block measured the surface roughness using a 3D non-contact profilometer with a 90º traverse direction (perpendicular to the building direction. Therefore, each face was already measured with five-time and considered good average data. This measurement can determine whether each face has a consistent surface roughness or not.

3D non-contact profilometer used to measure all faces surface roughness of block. The software used for measuring surface roughness is Winroof 2015, which is suitable for capturing the best image with automatic merge by software. Besides, this software is more accessible to measure the area we want and easy to get the average data of R_a (surface roughness) by duplicating the measurement area for a single image.

3.0 RESULTS AND DISCUSSION

3.1 Tensile Strength

Figure 5 shows that the samples already fractured after the test under the Instron 8872 machine. Table 2 summarizes the parameters used for the experiments. Therefore, the layer thickness was varied between 0.1 mm, 0.2mm, and 0.3 mm, and the infill density used was 0%. The selection of these machine parameters is due to the machine's limitation in the experiment and early exploration of these parameters' effect on the surface roughness. Nine averages of specimens result from the tensile strength using a different gas and layer thickness levels shown in Table 2. In the meantime, the data is already repeated four times to get an average for one specimen as in Table 2..

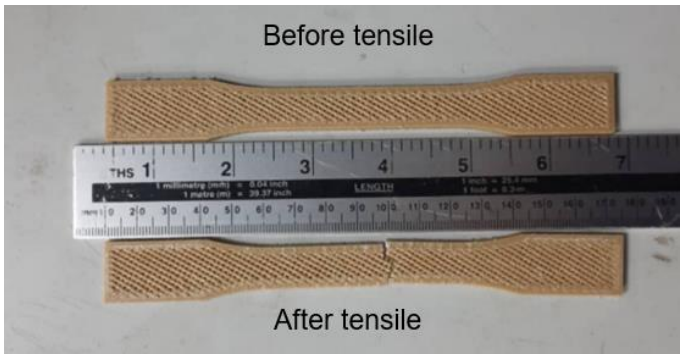

Figure 5: Fractured sample before (above) and after (below) tensile test.

Table 2: Summary result tensile strength for all dog bone samples.

Specimen number	Oxygen gas level (%)	Layer thickness (mm)	The average number of tensile Strength (MPa)
1		0.1	11.767
2	0	0.2	13.740
3		0.3	15.681
4		0.1	10.454
5	10	0.2	13.143
6		0.3	14.127
7		0.1	10.295
8	20	0.2	13.538
9		0.3	15.200

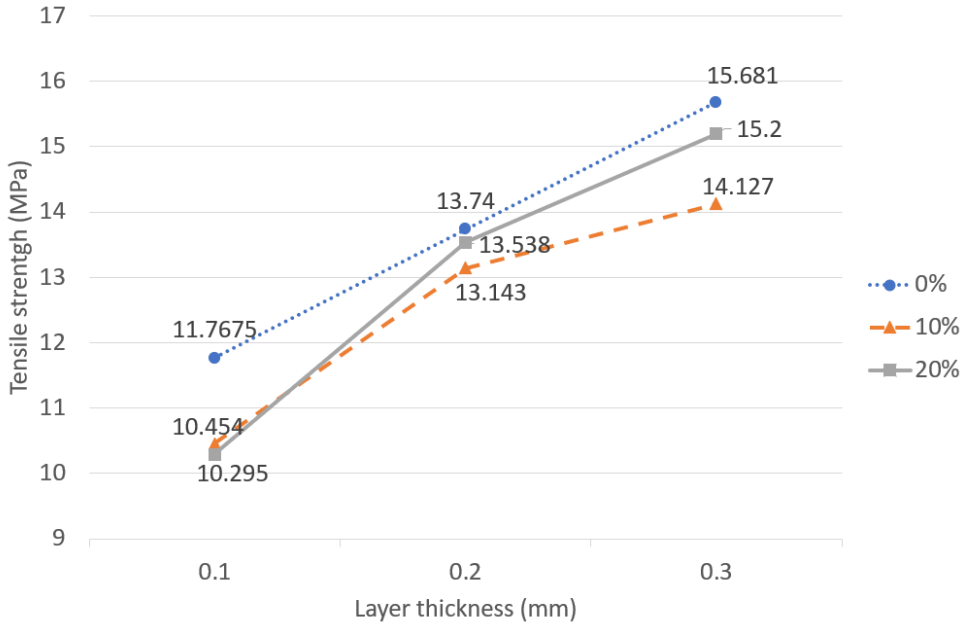

Figure 6: The effect of layer thickness on tensile strength with different levels of oxygen.

Figure 6 shows the tensile strength at the break of the sample dog bone with different layer thickness and oxygen levels. The average tensile strength increases with increasing layer thickness for all oxygen levels (0%, 10% and 20%). The 0% oxygen level has the best tensile strength result compared to 10% and 20% condition for all layer thickness, especially at 0.1mm layer thickness. Lower tensile strengths were obtained for 10% and 20% oxygen level since both conditions still contained oxygen in the 3D printing chamber and thus oxidation weakened the strength and the bonding of the printed parts. Due to several 3D printed dog bone samples tested, the average tensile strength for 10% and 20% oxygen level for layer thickness of 0.2mm and 0.3mm showed variation in the results. However, the difference of average tensile strength between 10% and 20% oxygen level is quite small especially if looking at the 0.1mm layer thickness results. An assumption can be made that by varying oxygen levels of 10% and 20%, they do not really affect the average tensile strength.

Tymrak et al., (2014) calculated that samples with the maximum layer thickness had the highest elastic modulus, while samples with the most negligible layer thickness had the highest tensile strength. They also speculated that the loss of strength is due to the vast heating and cooling cycles and the resulting residual stresses. Other types of 3D printing techniques have also investigated the effects of layer thickness (Vaezi & Chua, 2011). 0% infill density in this experiment, has a high layer thickness will enhance tensile strength. Nevertheless, 0% infill density will not be too rigid when comparing the samples with high filling density inside the sample to make it is more potent.

The data obtained from the tensile tests in Figure 6 shows that oxygen exclusion compared to those printed under a nitrogen atmosphere allows for improved mechanical properties for prints performed under the nitrogen gas atmosphere. The smaller layer thickness samples are tightly stapled, providing a stronger inter-layer bond relative to the large layer thickness samples. For

smaller layer thickness, samples can make the tensile strength high. However, microvoids within these layers gradually act as tension increases and reduce net tensile strength. Inter-layer bonding is weak with larger microvoids at a higher layer thickness, resulting in a lower tensile strength. The same explanation can be applied to a percentage decline in elongation (Che Mat et al., 2020).

3.2 Surface Roughness

Table 3 shows the result surface roughness for all samples block with different faces. Therefore, 3D contact non-profilometer was used for this experiment to get surface roughness data generated by a computer. Besides, data were repeated three times to get average data for every face.

Figure 7, Figure 8 and Figure 9 shows the surface roughness results for 0%, 10% and 20% oxygen respectively. The graphs trends for 0% and 10% are almost similar, where layer thickness of 0.1mm and 0.3mm has a higher value of R_a compared to layer thickness of 0.2mm. The non-existence oxygen or lack of oxygen in the chamber, produces samples that have slightly better, more stable, and relevant surface roughness. This is different from the results in Figure 9 when 20% oxygen (which is almost the same content of oxygen in air) was tested. The result confirms to the results obtain by Yan (2017), that the higher the layer thickness, the higher the surface roughness value. The differences of trend are apparent due to the oxidation and thermal degradation factors.

During 3D printing process, the polymer long-chain backbones components started to detach at high temperatures and reacted to alter the polymer properties with one another. This process was supposed to occur as the filament absorbed ambient humidity and became oxidized. One of the limiting factors of high-temperature plastic use is their propensity to become thinner and thermal degradation lead to loss of mechanical properties. As stated previously, the surface roughness improved due to a better adhesion layer and influenced the surface profile data. The melted filament had a strong bond, and well melted within the inert gas controlled the temperature of the melted filament between the particles. If thermal degradation can be managed, a superior adhesion layer can be created by suppressing the oxidation process during 3D printing. Thus, lower oxygen levels give more stable condition and layer thickness of 0.2mm can be assumed to be a reasonable layer thickness at this more stable state.

In addition, all faces (Face1-Face4) of the testing samples have variation results of R_a showing that the layers' deposition of the 3D printing filament does not influence the surface roughness results. This also may be affected by the performance of the open-source 3D printer, Anet A8 used in the experiment. The cracking effect was not apparent from the current experiment, but the component's surface was rough due to the bubble forming on the top surface. In the case of ABS material used in the experiments, the oxidation phase in the presence of oxygen resulted in polymer deterioration at a higher temperature. The oxidation process affected the polymer chemical reaction, which resulted in a significant decrease in mechanical properties. The polymer filament was melted during the FFF process at a comparatively high temperature between 235°C-240°C and layering on the printing bed. The molten polymer was exposed to the air during the printing process. Consequently, each layer's polymer surface is weakened as the layer-by-layer cycle affects mechanical properties.

Table 3: Summary result for all sampled blocks with different faces and oxygen concentration.

Specimen numbers	Face of cube	Oxygen gas level (%)	Layer thickness (mm)	The average number of R_a (µm)
1			0.1	15.6
2		0	0.2	14.6
3			0.3	12.8
4			0.1	27.2
5	Face no.1	10	0.2	8.4
6			0.3	21.2
7			0.1	21.4
8		20	0.2	23.1
9			0.3	25.3
10			0.1	19.6
11		0	0.2	10.2
12			0.3	14.9
13			0.1	25.5
14	Face no.2	10	0.2	9.1
15			0.3	23.5
16			0.1	17.2
17		20	0.2	14.2
18			0.3	14.3
19			0.1	19.8
20		0	0.2	14.0
21			0.3	15.3
22			0.1	27.2
23	Face no.3	10	0.2	10.0
24			0.3	28.9
25			0.1	25.5
26		20	0.2	16.8
27			0.3	25.3
28			0.1	8.2
29		0	0.2	16.6
30			0.3	14.5
31			0.1	24.7
32	Face no.4	10	0.2	9.4
33			0.3	30.5
34			0.1	18.3
35		20	0.2	16.9
36			0.3	21.2

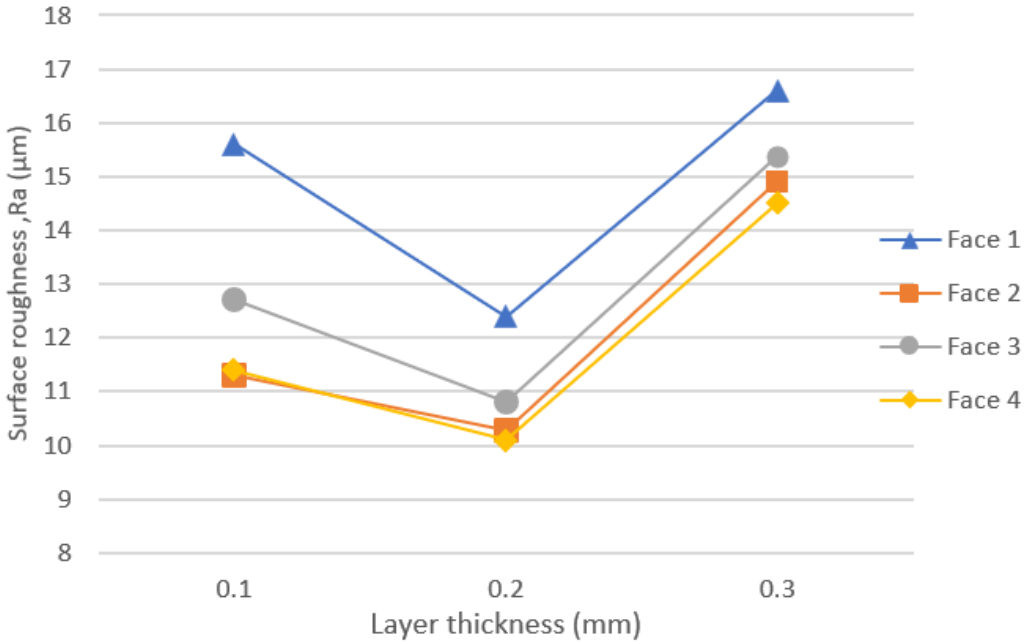

Figure 7: The effect of layer thickness on surface roughness with different faces at 0% oxygen contain.

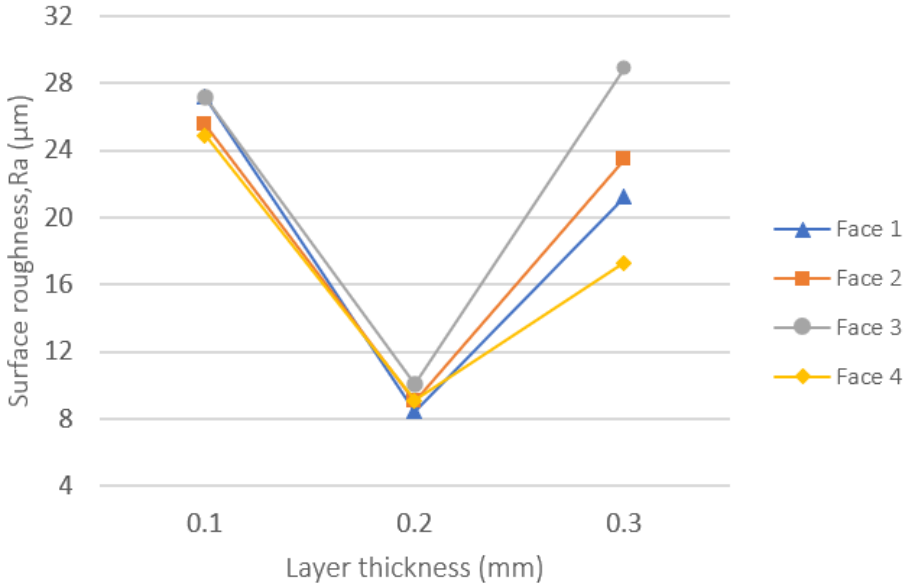

Figure 8: The effect of layer thickness on surface roughness with different faces at 10% oxygen contain.

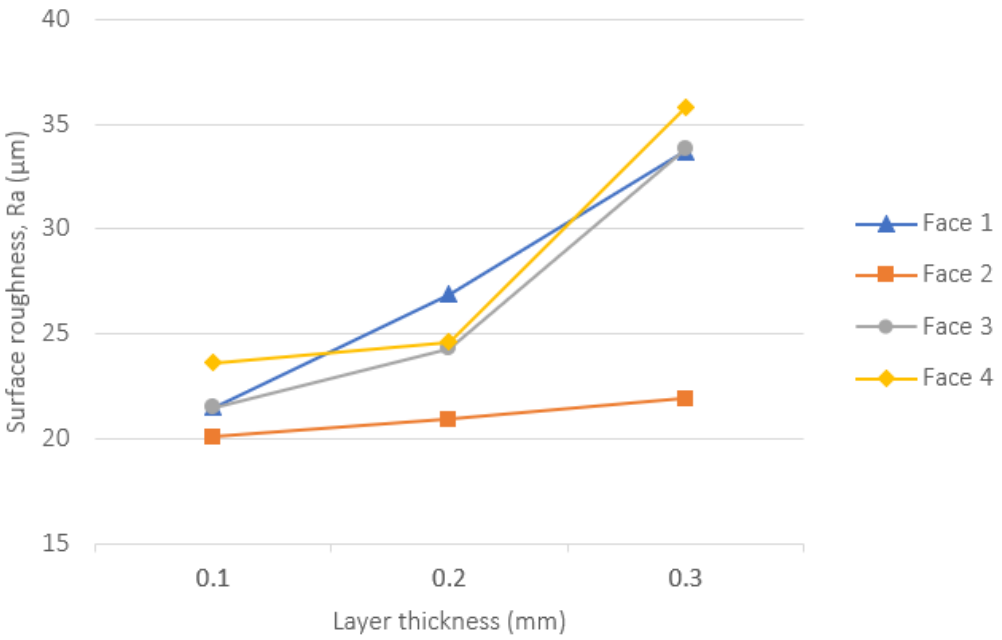

Figure 9: The effect of layer thickness on surface roughness with different faces at a 20% oxygen level.

3.3 The Surface Morphology of FFF Parts

The SEM was used to investigate the surface morphologies of FFF components. Therefore, Figure 10 shows the 0%, 10%, and 20% oxygen levels with 0.1mm layer thickness. Besides, Figure 10 (a) explains the strongest tensile strength with 11.767 (MPa) compared to Figure 10 (b) and (c) with 10.454 (MPa) and 10.295 (MPa). Furthermore, the specimens demonstrate a smooth fracture surface for Figure 10 (a), and the surface looks brittle for Figures 10 (b) and (c), which is a rougher surface. Moreover, the small voids area appears in Figure 10 (a) and is not too critical such as in Figures 10 (b) and (c), which has too many voids' areas. A slight air gap is required to form a tight bond between two rasters, thus increasing strength. This incident happens because by reducing the oxygen, oxidation also decreases, which is a high oxidation tendency to reduce a sample's molecular weight (Lederle et al., 2016).

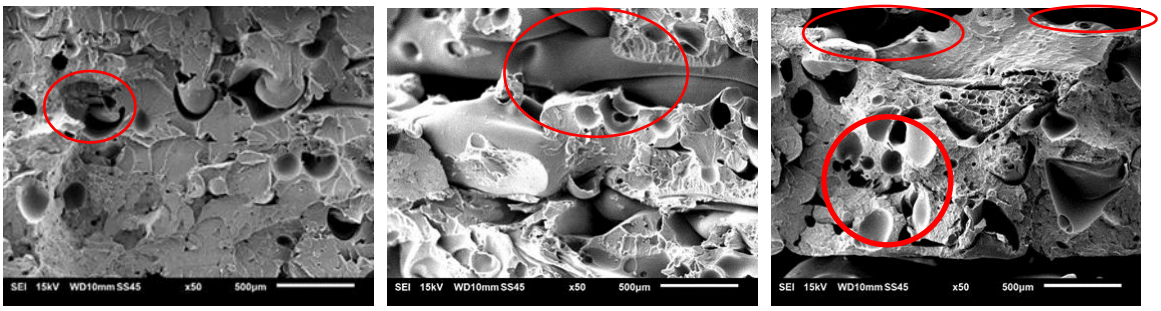

(a) 0% (b) 10% (c) 20%

Figure 10: SEM micrographs of the fracture surfaces of FFF specimens with layer thickness 0.1mm and increasing the concentration level of oxygen.

Figure 11 shows the FFF component's microstructure morphologies with a 0% oxygen level and increasing the layer thickness, as Figure 11 above. Figure 11 (a) shows the highest tensile strength with 15.681 (MPa) compared to (b) and (c) with 11.767 and 13.740 (MPa). These results can conclude that the higher the value of layer thickness, the higher the tensile strength value. In addition, the surface looks smoother with increasing the layer thickness in Figure 11. Similarly, the void area is also decreasing when increasing the layer thickness. The poor interlayer bonding for Figure 11 (a) explained that the decline in strength and distortion occurs due to the high-temperature gradient towards the bottom layers. If the layer thickness increases, fewer layers are needed, and the distortion effect reduces, resulting in increased strength (Wang et al., 2007).

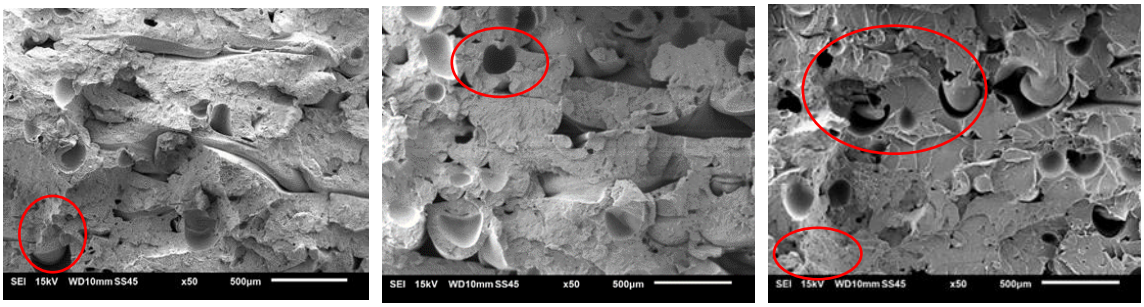

a) 0.1mm (b) 0.2mm (c) 0.3mm

Figure 11: SEM micrographs of FFF specimens fracture surfaces with 0% oxygen concentration with increasing layer thickness.

CONCLUSION

Based on this study, by controlling the oxygen level in 3D printing chamber, the tensile strength of 3D printed part has shown slight improvement with oxygen exclusion. However, varying different oxygen concentrations of 10% and 20%, do not produce significant improvement results. In addition, the surface roughness also shown improvement with lower oxygen content or with the absent oxygen in the chamber. In other words, excluding oxygen from the 3D printed chambers produced better tensile strength and surface roughness.

This experimental study also develops or improve the FFF method of improving printed part's quality and manufacturability using an open-source 3D printer. FFF process fabricates parts layer-by-layer, resulting in a poor quality of printed parts compared to other AM techniques. Besides, to enhance good surface quality, some methods and improvements by the inert gas (nitrogen) assisted the printing process, flooding the ambient of the printing chamber with nitrogen (N^2) to reduce and remove oxygen (O^2) from the surrounding chamber. The in-processing method with inert gas assist is conducted to control the temperature variable, so the layer's bonding is well melted and placed. Additionally, thermal degradation can be reduced to get better mechanical properties of the printed parts.

ACKNOWLEDGMENT

This study is supported by the Ministry of Education Malaysian FRGS/2018/FKM-CARE/F00369. The authors also acknowledge the use of the services and facilities of the Universiti Teknikal Malaysia Melaka.

REFERENCES

Ahn, S. H., Montero, M., Odell, D., Roundy, S., & Wright, P. K. (2002). Anisotropic material properties of fused deposition modeling ABS. Rapid Prototyping Journal, 8(4), 248–257.

Alafaghani, A., Qattawi, A., Alrawi, B., & Guzman, A. (2017). Experimental Optimization of Fused Deposition Modelling Processing Parameters: A Design-for-Manufacturing Approach. Procedia Manufacturing, 10, 791–803. https://doi.org/10.1016/j.promfg.2017.07.079

Alsoufi, M. S., & Elsayed, A. E. (2017). How Surface Roughness Performance of Printed Parts Manufactured by Desktop FDM 3D Printer with PLA+ is Influenced by Measuring Direction. American Journal of Mechanical Engineering, 5(5), 211–222.

Balashanmugam, N., Ankit, K., Aloysius, D., Sudha, L., Suresh, R. S., Krishna, P., & Shashikumar, P. V. (2014). STL-less based CAD/CAM Approach for Laser Scanning in Micro Stereo Lithography. Procedia Materials Science, 5, 1466–1472.

Buj-Corral, I., Domínguez-Fernández, A., & Durán-Llucià, R. (2019). Influence of print orientation on surface roughness in fused deposition modeling (FDM) processes. Materials, 12(23).

Che Mat, M., Redza Ramli, F., Rizal Alkahari, M., Nizam Sudin, M., Fadzli Bin Abdollah, M., Mat, S., & Kejuruteraan Mekanikal, F. (2020). Influence of layer thickness and infill design on the surface roughness of PLA, PETG and metal copper materials. December, 64–66.

D'Amico, A. A., Debaie, A., & Peterson, A. M. (2017). Effect of layer thickness on irreversible thermal expansion and interlayer strength in fused deposition modeling. Rapid Prototyping Journal, 23(5), 943–953.

Derby, B. (2011). Inkjet printing ceramics: From drops to solid. Journal of the European Ceramic Society, 31(14), 2543–2550. https://doi.org/10.1016/j.jeurceramsoc.2011.01.016

Diegel, O., Kristav, P., Motte, D., & Kianian, B. (2016). Handbook of Sustainability in Additive Manufacturing. 73–99.

Ferrar, B., Mullen, L., Jones, E., Stamp, R., & Sutcliffe, C. J. (2012). Gas flow effects on selective laser melting (SLM) manufacturing performance. Journal of Materials Processing Technology, 212(2), 355–364.

Fina, F., Goyanes, A., Gaisford, S., & Basit, A. W. (2017). Selective laser sintering (SLS) 3D printing of medicines. International Journal of Pharmaceutics, 529(1–2), 285–293.

Gajdoš, I., Spišák, E., Kaščák, Ľ., & Krasinskyi, V. (2015). Surface finish techniques for FDM parts. Materials Science Forum, 818(1), 45–48.

Galantucci, L. M., Bodi, I., Kacani, J., & Lavecchia, F. (2015). Analysis of dimensional performance for a 3D open-source printer based on fused deposition modeling technique. Procedia CIRP, 28, 82–87.

Galantucci, L. M., Lavecchia, F., & Percoco, G. (2010). Quantitative analysis of a chemical treatment to reduce roughness of parts fabricated using fused deposition modeling. CIRP Annals - Manufacturing Technology, 59(1), 247–250.

Gibson, I., Rosen, D., Stucker, B., & Khorasani, A. (2020). Additive Manufacturing Technologies. 10.1007/978-3-030-56127-7.

Hossain, M. S., Espalin, D., Ramos, J., Perez, M., & Wicker, R. (2014). Improved Mechanical Properties of Fused Deposition Modeling-Manufactured Parts Through Build Parameter Modifications. Journal of Manufacturing Science and Engineering, Transactions of the ASME, 136(6).

Lederle, F., Meyer, F., Brunotte, G. P., Kaldun, C., & Hübner, E. G. (2016). Improved mechanical properties of 3D-printed parts by fused deposition modeling processed under the exclusion of oxygen. Progress in Additive Manufacturing, 1(1–2), 3–7.

Li, J. (2008). Interfacial studies on the O 3 modified carbon fiber-reinforced polyamide 6 composites. Applied Surface Science, 255(5 PART 2), 2822–2824.

Li, J., & Cai, C. L. (2011). The carbon fiber surface treatment and addition of PA6 on tensile properties of ABS composites. Current Applied Physics, 11(1), 50–54.

Maidin, S., Mohamed, A. S., Akmal, S., Mohamed, S. B., Wong, J. H. U., Teknikal, U., Sultan, U., & Abidin, Z. (2018). Feasibility study of vacuum technology integrated fused deposition modeling to reduce staircase effect. Journal of Fundamental and Applied Science, 13.

Montes-Morán, M. A., Martínez-Alonso, A., Tascón, J. M. D., Paiva, M. C., & Bernardo, C. A. (2001). Effects of plasma oxidation on the surface and interfacial properties of carbon fibres/polycarbonate composites. Carbon, 39(7), 1057–1068.

N. Searle. (2014). Harmonization and Optimization of Weathering Test Methods for Building and Construction Sealants and Adhesives. Ournal of ASTM International 1, no. 3, 1–17.

Nazan, M. A., Ramli, F. R., Alkahari, M. R., Sudin, M. N., & Abdullaah, M. A. (2017). Process parameter optimization of 3D printer using Response Surface Method. ARPN Journal of Engineering and Applied Sciences, 12(7), 2291–2296.

Norani, M. N. M., Abdullah, M. I. H. C., Abdollah, M. F. Bin, Amiruddin, H., Ramli, F. R., & Tamaldin, N. (2021). Mechanical and tribological properties of fff 3d-printed polymers: A brief review. Jurnal Tribologi, 29(April), 11–30.

Nur, S., Mazlan, H., Alkahari, M. R., Maidin, N. A., Ramli, F. R., & Sudin, M. N. (2018). Influence of inert gas assisted 3D printing machine on the surface roughness and strength of printed component. May, 154–155.

Pérez, M., Medina-Sánchez, G., García-Collado, A., Gupta, M., & Carou, D. (2018). Surface quality enhancement of fused deposition modeling (FDM) printed samples based on the selection of critical printing parameters. Materials, 11(8).

Quadrennial Technology Review. (2015). Innovating Clean Energy Technologies in Advanced Manufacturing. U.S. Department of Energy.

Quan, Zhenzhen, Jonghwan Suhr, Jianyong Yu, X. Q., & Chase Cotton, Mark Mirotznik, and T.-W. C. (2018). "Printing Direction Dependence of Mechanical Behavior of Additively Manufactured 3D Preforms and Composites." Composite Structure, 184, 917–923.

Reddy, V., Flys, O., Chaparala, A., Berrimi, C. E., Amogh, V., & Rosen, B. G. (2018). Study on surface texture of Fused Deposition Modeling. Procedia Manufacturing, 25, 389–396.

Shubham, P., Sikidar, A., & Chand, T. (2016). The influence of layer thickness on mechanical properties of the 3D printed ABS polymer by fused deposition modeling. Key Engineering Materials, 706(2), 63–67.

Sood, A. K., Ohdar, R. K., & Mahapatra, S. S. (2010). Parametric appraisal of mechanical property of fused deposition modelling processed parts. Materials and Design, 31(1), 287–295.

Tymrak, B. M., Kreiger, M., & Pearce, J. M. (2014). Mechanical properties of components fabricated with open-source 3-D printers under realistic environmental conditions. Materials and Design, 58, 242–246.

Vaezi, M., & Chua, C. K. (2011). Effects of layer thickness and binder saturation level parameters on 3D printing process. International Journal of Advanced Manufacturing Technology, 53(1–4), 275–284.

Wang, T. M., Xi, J. T., & Jin, Y. (2007). A model research for prototype warp deformation in the FDM process. International Journal of Advanced Manufacturing Technology, 33(11–12), 1087–1096.

Yan, J., Battiato, I., & Fadel, G. (2017). Design of injection nozzle in direct metal deposition (DMD) manufacturing of thin-walled structures based on 3D models. International Journal of Advanced Manufacturing Technology, 91(1–4), 605–616. https://doi.org/10.1007/s00170-016-9773-z

Yuen, P. K. (2016). Embedding objects during 3D printing to add new functionalities. Biomicrofluidics, 10(4), 9–12.